Submitted to the 29th International Conference on High-Energy Physics ICHEP98,
Vancouver, Canada, July 1998

# SEARCH FOR EXCITED FERMIONS AT HERA

H1 Collaboration

**Abstract**

We present a search for excited fermions in $e^+p$ scattering at HERA using H1 data with an integrated luminosity of 37 pb$^{-1}$. All electroweak decays of excited leptons, $\ell^* \rightarrow \ell\gamma, \ell W, \ell Z^0$ are considered. The excited quarks are searched for in the $q^* \rightarrow q\gamma$ and $qW$ channels. The analysis considers $Z^0$ and $W$ hadronic decays and first generation leptonic decays. No evidence for new particle production is found. Mass dependent exclusion limits on cross sections and coupling constants are derived.

**Abstract: 581**
**Parallel sessions: 10**
**Plenary sessions: 12**

# 1 Introduction

Convincing evidence for a substructure of fermions could be the discovery of excited quarks and leptons. Electron-proton interactions at very high energies provide an excellent environment to look for excited fermions of the first generation. At the $ep$ collider HERA magnetic-transition couplings of the positron to a gauge boson would allow single production of $e^*$ through $t-$channel $\gamma$ and $Z$ boson exchange or single production of $\nu^*$ through $t-$channel $W$ boson exchange. In the same way excited quarks could be produced through $t-$channel gauge boson exchange between the incoming positron and a quark of the proton.

In this paper we report on a search for excited fermions using the $e^+p$ data accumulated by the H1 experiment at HERA from 1994 to 1997 and corresponding to an integrated luminosity of 37 pb$^{-1}$. The positron and proton beam energies were respectively equal to 27.5 $\mathrm{GeV}$ and 820 $\mathrm{GeV}$. The excited leptons are studied through all their decays into a lepton and a gauge boson and the excited quark analysis concentrates on the main decays, $q^* \to q\gamma$ and $q^* \to qW$. The subsequent gauge bosons ($W$ and $Z^0$) decays studied are those involving electrons [1], neutrinos or jets. This study corresponds to a statistical increase of more than a factor 10 compared to previous H1 searches [1, 2, 3].

The paper is organized as follows. After a short description of the H1 detector and of our preselection in section 2, we present briefly in section 3 the events generators used. Section 4 contains the analysis description. The results and their comparison with a similar analysis done by the ZEUS collaboration [4] are reported in section 5. Comparisons with limits obtained on excited leptons by the LEP experiments [5, 6, 7] and on excited quarks by the Tevatron experiments [8, 9] are also shown. Finally, section 6 summarizes the results.

# 2 The H1 detector

A full description of the H1 detector can be found in reference [10]. Here we describe briefly the components which are relevant for this analysis. The interaction region is surrounded by a drift chamber and proportional chamber tracking system covering the angular range $7^o < \theta < 176^o$ (the forward direction, $z$ >0, from which the polar angle $\theta$ is measured is the proton beam direction). The tracking system is placed into a finely segmented liquid argon calorimeter covering the polar angular range $4^o < \theta < 154^o$. The electromagnetic part is made of lead/argon and the hadronic part of stainless steel/argon [11]. For the LAr calorimeter energy resolution of $\frac{\sigma_E}{E} = \frac{12\%}{\sqrt{E}} \oplus 1\%$ for electrons and $\frac{\sigma_E}{E} = \frac{50\%}{\sqrt{E}} \oplus 2\%$ for hadrons have been obtained in test beam measurements [12, 13]. A lead-scintillating fiber calorimeter is located in the backward region ($154^o < \theta < 178^o$) of the H1 detector [14] [2]. The tracking system and calorimeters are surrounded by a super-conducting solenoid producing a uniform field of 1.15 T in the $z$ direction.

The analysis uses the $e^+p$ data accumulated over periods in which the main H1 components, the central jet chambers, the LAr calorimeter, and the luminosity system were fully operational. The preselection of events relies on the requirement of at least one high $E_t$ electromagnetic shower or missing transverse energy. Background not related to $e^+p$ collisions is rejected by requiring that the event time coincides with that of the bunch crossing, using topological filters, and by requesting a primary vertex within $\pm 35$ cm of the nominal vertex value.

[1]The term 'electron' stands generically for electron or positron.
[2]This detector has replaced in 1995 a conventional lead-scintillator sandwich calorimeter [15].

# 3 Generators

The main Standard Model backgrounds which could mimic the above signatures are neutral current Deep Inelastic Scattering (NC DIS), charged current Deep Inelastic Scattering (CC DIS), QED Compton scattering and photoproduction processes.

Backgrounds from CC DIS and NC DIS are simulated using the event generator DJANGO [16] which includes QED first order radiative corrections and real bremsstrahlung photons based on HERACLES [17]. QCD radiation is implemented using ARIADNE [18] and the hadronic final state is generated according to the string fragmentation model by JETSET [19]. QED compton scattering events are simulated with the event generator EPCOMPT [20] and compared to the predictions of an other QED Compton event generator COMPTON2.0 [21] (see section 5.1). The inelastic process $ep \to e\gamma X$ is taken into account in both generators NC DIS (radiative events) and QED Compton scattering. To avoid a double counting, we used the QED Compton program to generate events with a negative squared four momentum transferred $Q^2$ from the incoming proton to the final hadronic state below 100 $\mathrm{GeV}^2$ and the NC DIS one above. The effect of using or not this $Q^2$ criterion is taken into account as a systematic error (section 5.1). The MRS H [22] parton distributions in the proton are used for the inelastic scattering. Direct and resolved photoproduction processes, including prompt photon production are simulated with the PYTHIA Monte Carlo [23] event generator. Others processes, corresponding to much lower cross sections, such as $\gamma\gamma$ interactions or $W$ production have also been simulated. The $\gamma\gamma$ process is simulated using the LPAIR generator [24] and the $W$ simulation is studied with the EPVEC program [25]. The luminosities generated for these Monte Carlos are varying between 3 times to 100 times the experimental luminosity.

In order to calculate the acceptance of our selection criteria, a Monte Carlo simulation of excited fermion production and decay is necessary. This analysis uses the COMPOS [26] generator which is based on the cross section described in [27] for $l^*$ production and was modified, for $q^*$ generation, following the cross section given in [28].

All Monte Carlo generators are interfaced to a full simulation of the H1 detector response.

# 4 Search for Excited Fermions

In this section we describe the analysis according to the experimental signatures of the final states.

## 4.1 Final states with no missing transverse momentum

When only particles in the proton direction remain undetected, longitudinal momentum conservation implies that the variable $\sum_i(E_i - P_{z_i})$, where $E_i$ and $P_{z_i}$ are the energy and the longitudinal momentum in a calorimeter cell $i$, has to be equal to 2 times the energy of the incoming positron. Therefore we apply the cut: (35 $\mathrm{GeV} < \sum_i(E_i - P_{z_i}) <$ 65 $\mathrm{GeV}$) in the following studies unless otherwise stated. This cut rejects photoproduction and CC DIS backgrounds.

#### 4.1.1 Events with 2 electromagnetic clusters : the $e^* \rightarrow e\gamma$ channel

The $e^* \rightarrow e\gamma$ decay mode is the most distinct channel in which to search for $e^*$ because of its high branching ratio ($\simeq 30\%$ is expected for $e^*$ masses above 150 $\mathrm{GeV}$ [29]) and its very clear signature. The main backgrounds are the QED Compton process with a well separated $e - \gamma$ pair in the final state, NC DIS with photon radiation or an isolated $\pi^0$ and the two-photon ($\gamma\gamma$) production of electron pairs, the latter being found to be small.

- Exclusive analysis:
  It has been shown [27] that about half of the cross section is expected in the elastic channel $ep \rightarrow e^*p$. In this case the signature consists of only two electromagnetic clusters and nothing else in the detector. The remaining source of background left is the QED Compton scattering, the NC DIS background being strongly suppressed by the requirement of no other signals in H1. The selection is described in table 1. We require 2 isolated electromagnetic clusters with a total energy above 20 $\mathrm{GeV}$ (cuts 1 and 2). The requirement 3, where $M_{12}$ is the invariant mass of the 2 electromagnetic clusters, reduces the QED Compton background which is at predominantly low electron-photon masses. Requirements 4 and 5 are loose cuts and use the fact that for $(e^* \rightarrow e\gamma)$ and QED Compton processes the kinematics are over-constrained. Using the polar angles of the 2 electromagnetic clusters alone, their energies and the invariant mass can be computed and compared to the measured quantities $E_i$ and $M_{12}$. Requirement 6 is the empty detector condition, where $E_{tot}$ is the total energy deposited in the calorimeter.
  After application of the above cuts 319 events remain. The expectation from Standard Model processes is $339 \pm 7$ (336 QED Compton and 3 $\gamma\gamma$). The average efficiency of this selection for $e^*$ masses above 50 $\mathrm{GeV}$ is equal to $47\%$.

| | |
|---|---|
| 1 | $\geq$ 2 isolated e.m clusters, $E_i >$ 5 $\mathrm{GeV}$ and $10^o < \theta_i < 150^o$ |
| 2 | $E_1 + E_2 >$ 20 $\mathrm{GeV}$ |
| 3 | $M_{12} >$ 10 $\mathrm{GeV}$ |
| 4 | $\lvert M(\theta_1, \theta_2) - M_{12} \rvert < 2\ M_{12}$ |
| 5 | $\lvert E_i(\theta_1, \theta_2) - E_i \rvert < E_i$ |
| 6 | $E_{tot} - E_1 - E_2 <$ 5 $\mathrm{GeV}$ |

Table 1: Selection requirements for the exclusive analysis.

- Inclusive analysis:
  To improve the acceptance, at least for $e^*$ masses above 50 $\mathrm{GeV}$, we relax the empty detector condition and require events with 2 high $E_t$ isolated electromagnetic clusters ($E_{t_i} \geq 20$ and $10$ $\mathrm{GeV}$ and $\theta_i \leq 150^o$). To reduce the NC DIS contribution with an isolated $\pi^0$, a cut on the multiplicity of tracks pointing to the electromagnetic cluster is made.
  After this selection $223$ candidates are selected and the expected Standard Model background is $239 \pm 6$ events ($76$ QED Compton, $161$ NC DIS and $2$ $\gamma\gamma$).

The combined efficiencies of the two selections for $e^* \rightarrow e\gamma$ are given in table 2, as well as those of all other channels described hereafter. The 2 electromagnetic clusters invariant masses of the candidates are shown in figures 1 and 2 for the exclusive and inclusive analyses respectively, together with the expected background for each of the 2 selections. The shapes of the data distributions and the predictions of the Standard Model are in good agreement.

#### 4.1.2 Events with more than 2 electromagnetic clusters : the $e^* \to eZ_{\hookrightarrow ee}$ channel

Using the sub-sample of events with 2 high $E_t$ electromagnetic clusters, a third electromagnetic cluster with $E_t \geq 5$ GeV and $\theta \leq 150^o$ is requested. An additional cut, to reduce NC DIS background, rejects events having a jet with $E_t$ above 15 GeV, jets being defined using a cone algorithm of radius $R = 1$ in the $\eta - \phi$ plane. After this selection 3 events are left while $(1.4 \pm 0.3)$ background events are expected (0.7 from NC DIS and 0.7 from $\gamma\gamma$).

| M($f^*$) GeV | 25 | 50 | 75 | 100 | 150 | 200 | 250 |
|---|---|---|---|---|---|---|---|
| $e^* \to e\gamma$ | 24 | 65 | 84 | 86 | 85 | 83 | 79 |
| $\nu^* \to \nu\gamma$ | - | 27 | 46 | 50 | 41 | 36 | 23 |
| $q^* \to q\gamma$ | - | 23 | 34 | 37 | 43 | 43 | 41 |

| M($f^*$) GeV | 95 | 120 | 150 | 200 | 250 |
|---|---|---|---|---|---|
| $e^* \to eZ_{\hookrightarrow ee}$ | $< 1$ | 76 | 77 | 78 | 76 |
| $e^* \to eZ_{\hookrightarrow \nu\bar{\nu}}$ | $< 1$ | 7 | 71 | 79 | 81 |
| $e^* \to eZ_{\hookrightarrow q\bar{q}}$ | $< 1$ | 49 | 50 | 41 | 37 |
| $e^* \to \nu W_{\hookrightarrow e\nu}$ | 63 | 64 | 64 | 56 | 54 |
| $e^* \to \nu W_{\hookrightarrow q\bar{q}}$ | $< 1$ | 37 | 43 | 40 | 34 |
| $\nu^* \to \nu Z_{\hookrightarrow ee}$ | $< 1$ | 29 | 42 | 35 | 31 |
| $\nu^* \to \nu Z_{\hookrightarrow q\bar{q}}$ | 3 | 34 | 55 | 56 | 40 |
| $\nu^* \to eW_{\hookrightarrow e\nu}$ | 34 | 46 | 43 | 39 | 33 |
| $\nu^* \to eW_{\hookrightarrow q\bar{q}}$ | 35 | 47 | 49 | 39 | 28 |
| $q^* \to qW_{\hookrightarrow e\nu}$ | 3 | 38 | 42 | 43 | 37 |

Table 2: Selection efficiencies for different decay modes of the excited fermions $f^*$. They are given as percentages and based on 1000 simulated events per mass and per channel.

#### 4.1.3 Events with 2 high $E_t$ jets and one electromagnetic cluster: the $e^* \to eZ_{\hookrightarrow q\bar{q}}$ and $\nu^* \to eW_{\hookrightarrow q\bar{q}}$ channels

These channels are characterized by two high $E_t$ jets and an electromagnetic cluster. Background events are expected from NC DIS. A cone algorithm with a radius $R = 1$ in the $\eta - \phi$ plane is used to define the jets. At least 2 jets should have a transverse energy greater than 20 GeV, their polar angle greater than $10^o$ and a (jet-jet) invariant mass between 60 and 120 GeV. Candidates are selected if they have in addition an isolated electromagnetic cluster with $E_t \geq 10$ GeV and with $10^o < \theta < 100^o$ This cut on the transverse energy of the electromagnetic cluster induces an efficiency loss at $e^*$ masses close to the $Z$ mass (see table 2). The cut on the polar angle of the cluster discriminates signal from NC DIS background because of the boost due to high $f^*$ mass.

38 events are found for an estimated NC DIS background of 48 $\pm$ 3 events. The photoproduction, $W$ and $Z$ production backgrounds have been evaluated and found to be negligible compared to NC DIS. Figure 3 shows the invariant mass $M_{ejj}$ of the 2 jets and the electromagnetic cluster. No excess of events is found comparing to the Standard Model expectation.

### 4.1.4 Events with one photon and a jet : the $q^* \to q\gamma$ channel

The $q^*$ production is dominated by $\gamma$ exchange with small values of the squared momentum transfer so the scattered positron is often unseen in the detector. Hence the cut on the variable $\sum_i(E_i - P_{z_i})$ is not used for this channel. The final state is characterized by a photon and a jet. The main backgrounds come from photoproduction processes with prompt $\gamma$ production or with highly energetic $\pi^0$ and NC DIS events when the associated track with the scattered electron is not reconstructed. In this analysis we ask for one high $E_t$ isolated electromagnetic cluster ($E_t(\gamma) \geq 20$ GeV, $10^o < \theta(\gamma) < 90^o$) with no track pointing to it within a distance of 40 cm. We request a jet with $E_t > 15$ GeV and $\theta > 10^o$ and no electron with $E_t$ above 5 GeV in the LAr calorimeter. 35 events are selected compared to a background estimation of 34.3±5.7 events (2.6 NC DIS, 12.1 $\gamma p$, and 19.6 prompt photon). Figure 4 shows the distributions of the invariant $\gamma - jet$ masses for the data and the expected background. No significant excess is seen.

## 4.2 Final states with missing transverse momentum

In the analysis of channels involving a neutrino, a minimum missing transverse momentum $P_t^{miss}$ of 20 GeV is requested and the variable $\sum_i(E_i - P_{z_i})$ has to be less than 50 GeV. To remove events where the missing transverse momentum could come from fluctuations of the hadronic energy measurement, an additional cut for the channels with jets is made. A variable $P_t^{miss\perp}$ is defined as the maximum value of the projections of $P_t^{miss}$ perpendicular to any jet axis. The cut $P_t^{miss\perp} > 10$ GeV is applied.

### 4.2.1 Events with one photon, missing $P_t$ and a jet : the $\nu^* \to \nu\gamma$ channel

The final state contains an isolated electromagnetic cluster with no track pointing to it. As the $\nu^*$ is produced through $t$-channel $W$ boson exchange, most of the times the events contain also the recoil jet. The main background here are the CC DIS events and the NC DIS events with a large missing transverse momentum due to fluctuation of the hadronic shower. The selection criteria are one high $E_t$ isolated electromagnetic cluster ($E_t(\gamma) \geq 20$ GeV, $10^o < \theta(\gamma) < 100^o$) and a jet with $E_t > 5$ GeV.

All of the events which survived at this stage are found by visual inspection to be clear cosmic ray induced events, so no candidate is left. The expected Standard Model contribution is equal to 1.3 ± 0.7 events (0.7 NC DIS and 0.6 CC DIS).

### 4.2.2 Events with one electron, missing $P_t$ and a jet : the $q^* \to qW_{\hookrightarrow e\nu}$ channel

The main backgrounds in this channel are the same as in the paragraph 4.2.1 with in addition $W$ production. Cuts select events with one high $E_t$ electron ($E_{t_e} > 15$ GeV and $10^o < \theta_e < 150^o$) and a jet ($E_{t_j} > 15$ GeV and $\theta_j > 10^o$). One event survives the selection for an expected background of 1.4 ± 0.3 event (0.7 NC DIS, 0.5 $W$, 0.2 CC DIS).

#### 4.2.3 Events with 2 high $E_t$ jets and missing $P_t$: the $e^* \rightarrow \nu W_{\hookrightarrow q\bar{q}}$ and $\nu^* \rightarrow \nu Z_{\hookrightarrow q\bar{q}}$ channels

For this channel events with 2 jets having $E_t$ above 20 $\mathrm{GeV}$ , $\theta > 10^o$ and a di-jet invariant mass above 60 $\mathrm{GeV}$ are selected. Furthermore, to reduce the NC DIS background, events with an electron are rejected. 7 events are kept, with 4 of them identified as cosmic rays induced events after visual inspection. The background expectation is equal to 3.8 $\pm$ 0.5 events with 2.8 events from CC DIS, 0.8 event from photoproduction and 0.2 event from NC DIS.

#### 4.2.4 Events with 2 high $P_t$ electrons and missing $P_t$: the $\nu^* \rightarrow eW_{\hookrightarrow e\nu}$ and $\nu^* \rightarrow \nu Z_{\hookrightarrow e^+e^-}$ channels

The selection is based on 2 high $E_t$ electromagnetic clusters ( $E_{t_1}$ >20 $\mathrm{GeV}$ and $E_{t_2} >$ 10 $\mathrm{GeV}$ with $10^o < \theta_i < 150^o$) . A cut is applied on the $e\nu$ invariant mass in the search for the first channel, on the $ee$ invariant mass for the second one. No candidate has been found, the Standard Model expectation is 0.38 $\pm$ 0.16 event (0.12 $\gamma\gamma$, 0.16 QED Compton, 0.1 $W$).

#### 4.2.5 Events with 1 high $P_t$ electron and missing $P_t$: the $e^* \rightarrow \nu W_{\hookrightarrow e\nu}$ and $e^* \rightarrow eZ_{\hookrightarrow \nu\bar{\nu}}$ channels

The channel is characterized by only one electron having a large transverse momentum. The non $ep$ background ( cosmics and halo muons) is severe and we increase the minimum missing transverse momentum requirement from 20 to 25 $\mathrm{GeV}$. An isolated high $E_t$ electron ($E_{t_e} >$ 20 $\mathrm{GeV}$ with $10^o < \theta_e < 150^o$) and no jet with $E_t$ above 15 $\mathrm{GeV}$ are requested. This selection accepts 12 events. However after a visual inspection only one candidate is left. The expected background is equal to 3.6 $\pm$ 0.7 events (2 NC DIS, 0.8 $W$, 0.5 CC DIS, 0.2 QED Compton, 0.1 $\gamma\gamma$).

# 5 Results

## 5.1 Upper Limits on Excited Fermion production cross section

In the various channels considered in this analysis, the number of observed events are found to be in a good agreement with the predictions of the Standard Model. In addition no evidence is found for any discrepancy between Standard Model expectation for the relevant invariant mass distributions and measurement.

Therefore upper limits on the product of the $f^*$ production cross section and the decay channel branching ratio have been derived at the $95\%$ confidence level. These limits are determined as a function of the excited fermion mass. A mass window is displaced over the whole mass range with a step of 5 $\mathrm{GeV}$. The width of each window is chosen according to the resolution for the corresponding mass. In each mass interval, the number of observed events, the number of expected background events and the signal efficiency are determined and used to extract the upper limit for the signal following the prescription given in the Particle Data Group [30]. We take into account statistical and systematic errors in the contributions of the background and the efficiency by folding Gaussian distributions into the integration of the Poisson law used to determine the limit.

The errors taken into account on the background determination are the following:

- The errors due to the limited statistics of the Monte Carlo generations.
- An error on the absolute electromagnetic energy scale of $3\%$ and on hadronic energy scale of $5\%$.
- For the $e^* \to e\gamma$ search, two additional errors are taken into account. The QED Compton background expectations given by the 2 events generators [20, 21] are compared and found to be in good agreement. The difference of number of events is less than $10\%$ and is taken into account as a systematic error. The second error comes from the application or not of the $Q^2$ value when using together the QED Compton and the NC DIS generators to simulate the inelastic process $ep \to e\gamma X$ (see section 3).

and the errors taken into account on the efficiency determination are:

- A statistical uncertainty on the signal acceptance which varies between $3$ to $4\%$.
- For the radiative decays, the model dependence of the excited fermion angular decay distribution is taken into account by comparing the acceptance for isotropic decays to the distribution of the specific model used [3].

Finally an overall systematic error of $3\%$ on the luminosity is applied.

The effect of the systematic errors on the limit is given as percentages in table 3. The limit for the $l^*$ decaying in a lepton and a $W$ or a $Z$ is mainly given by the final states where the $W$ or $Z$ decays hadronically. The error is dominated by the uncertainty on the absolute calibration of the calorimeters for hadronic clusters, as it is for the $q^* \to q\gamma$ for $q^*$ masses below 75 $\mathrm{GeV}$. Concerning the $e^* \to e\gamma$, the main systematic error comes from the low $Q^2$ simulation at low masses ($\leq$ 50 $\mathrm{GeV}$) and is dominated by the electromagnetic scale uncertainty at higher masses.

<table>
<tr><th>M($f^*$) GeV</th><th>50</th><th>75</th><th>100</th><th>125</th><th>150</th><th>200</th><th>$>$ 200</th><th>#events</th></tr>
<tr><td>$e^* \to e\gamma$</td><td>45</td><td>20</td><td>15</td><td>10</td><td>6</td><td colspan="2">$<1$</td><td>482</td></tr>
<tr><td>$e^* \to eZ$</td><td>-</td><td>-</td><td>70</td><td>17</td><td>1</td><td colspan="2">$<1$</td><td>38</td></tr>
<tr><td>$e^* \to \nu W$</td><td>-</td><td>-</td><td>11</td><td>6</td><td colspan="3">$<1$</td><td>3</td></tr>
<tr><td>$\nu^* \to \nu\gamma$</td><td colspan="3">0.8</td><td>1</td><td>2</td><td>5</td><td>7</td><td>0</td></tr>
<tr><td>$\nu^* \to \nu Z$</td><td>-</td><td>-</td><td>16</td><td>12</td><td>6</td><td>3</td><td>$<1$</td><td>3</td></tr>
<tr><td>$\nu^* \to eW$</td><td>-</td><td>-</td><td>80</td><td>50</td><td>40</td><td>6</td><td>$<1$</td><td>38</td></tr>
<tr><td>$q^* \to q\gamma$</td><td>25</td><td colspan="3">10</td><td>9</td><td>1</td><td>3</td><td>35</td></tr>
<tr><td>$q^* \to qW$</td><td>-</td><td>-</td><td>1</td><td colspan="4">$<1$</td><td>1</td></tr>
</table>

Table 3: Effect of the systematic errors on the limit on the product of the cross section and the decay channel branching ratio. The values shown are: $R = \frac{limit\ with\ sys.err. - limit\ without\ sys.err.}{limit\ without\ sys.err.}$ They are given as percentages. The last column gives the number of events for the decay channel which contributes the most to the limit.

The limits on the product of the $f^*$ production cross section and the decay channel branching ratio are shown on figures 5, 6 and 7. These results improve by an order of magnitude earlier published H1 results [3].

[3]For $f^* \to f\gamma$ the distribution is $(1 + \cos\theta^*)$ where $\theta^*$ is the angle between the incoming and outgoing fermion in the $f^*$ rest frame.

### 5.2 Upper Limits on coupling parameters

We used a specific model [27, 28], in which the cross sections depend on coupling constants $f$, $f'$ and $f_s$ for the gauge groups $SU(2)$, $U(1)$ and $SU(3)$, and a substructure scale $\Lambda$. Assuming relations between $f$ and $f'$, branching ratios depend only on $\frac{f}{\Lambda}$ and constraints on these parameters can be derived. In figures 8 and 9 limits on the ratio $\frac{f}{\Lambda}$ are given for the $e^*$ and $\nu^*$ respectively. We assumed, as is conventional, $f = f'$ except for the $\nu^* \to \nu\gamma$ channel which is forbidden unless $f \neq f'$. For this decay we chose $f = -f'$. Values of $\frac{f}{\Lambda}$ above $0.6\ 10^{-3}$ $\mathrm{GeV}^{-1}$, for an $e^*$ mass equal to 60 $\mathrm{GeV}$, to $6\ 10^{-3}$ $\mathrm{GeV}^{-1}$, for an $e^*$ mass equal to 230 $\mathrm{GeV}$, are excluded. In the same way, the exclusion region of $\frac{f}{\Lambda}$ is above values varying between $0.3\ 10^{-2}$ to $9\ 10^{-2}$ $\mathrm{GeV}^{-1}$ for an $\nu^*$ mass interval of 60 to 185 $\mathrm{GeV}$.

The same analysis has been done for the $q^*$ where we assumed also $f = f'$ and that the $q^*$ has only electroweak couplings (i.e. $f_s = 0$)(see figure 10) . This last assumption is motivated by the results obtained by the Tevatron experiments [8, 9]. At the $p\overline{p}$ collider excited quarks are produced in a quark-gluon fusion mechanism which requires $f_s \neq 0$. Assuming $\Lambda = M(q^*)$, CDF excludes excited quarks in the HERA mass range (80-300 $\mathrm{GeV}$) for $f = f' = f_s$ value greater than 0.2.
Our exclusion region for $q^*$ masses between 60 to 230 $\mathrm{GeV}$ correspond to values of $\frac{f}{\Lambda}$ above $0.8\ 10^{-3}$ to $1.9\ 10^{-2}$ $\mathrm{GeV}^{-1}$.

The ZEUS experiment has published results based on their 94-95 $e^+p$ data for an integrated luminosity of 9.4 $\mathrm{pb}^{-1}$ [4]. Their limits, reported on figures 11, 12 and 13, are worse than those extracted from our analysis because we use a larger integrated luminosity. The $\nu^*$ cross section in $e^-p$ collisions is expected to be significantly higher than in $e^+p$ collisions. The $\nu^*$ ZEUS limit extracted from the $e^-p$ data [31] (integrated luminosity of 0.55 $\mathrm{pb}^{-1}$) is also shown on figure 12. It is better than the ZEUS limit obtained from $e^+p$ data for $\nu^*$ masses above 130 $\mathrm{GeV}$.

LEP experiments have also reported searches for excited leptons at $e^+e^-$ center of mass energies $\sqrt{s} = 161$ $\mathrm{GeV}$ [5], 170-172 $\mathrm{GeV}$ [6] and 183 $\mathrm{GeV}$ [7]. Excited leptons might be produced in pairs, then the limits are independent from the couplings parameters $f$ and $f'$. The best limits are given by the L3 experiment [7], excluding $e^*$ and $\nu^*$ with masses below 91.1 $\mathrm{GeV}$ and 89.5 $\mathrm{GeV}$ respectively at the 95% C.L. Single excited states might also be produced. Each of the four experiments, assuming $f = -f'$, gives limits for $\nu^*$ on the ratio $\frac{f}{\Lambda}$ of the order of 0.3 $10^{-2}$ to $10^{-1}$ $\mathrm{GeV}^{-1}$ for masses in the 80-170 $\mathrm{GeV}$ range. For the $e^*$, L3 gives the best limits which are of the order of 0.3 to 0.6 $10^{-3}$ $\mathrm{GeV}^{-1}$ for masses between 80 and 180 $\mathrm{GeV}$. LEP limits are compared to ours on figures 11 and 12.

## 6 Summary

Using data taken from 1994 to 1997 corresponding to an integrated luminosity of 37 $\mathrm{pb}^{-1}$, a search for production of excited fermions has been carried out in most of the possible decay channels. No evidence for excited fermions has been found in the channels which are the following, $e^* \to e\gamma$, $e^* \to eZ$, $e^* \to \nu W$, $\nu^* \to \nu\gamma$, $\nu^* \to \nu Z$, $\nu^* \to eW$, $q^* \to q\gamma$ and $q^* \to qW$.

New limits for the production of excited fermions in high energy positron proton interactions have been obtained, which improve previous H1 results by a factor 10. The exclusion domains of the coupling parameter $\frac{f}{\Lambda}$ and the excited fermion mass extends beyond that published by the ZEUS collaboration. Results obtained by the LEP experiments on $\frac{f}{\Lambda}$ for the $e^*$ and $\nu^*$ are more stringent but limited to excited leptons masses below 180 $\mathrm{GeV}$, so HERA extends the limits to higher masses. The results obtained on $q^*$ production are complementary to those given by the Tevatron experiments since the $q^*$ is produced via electroweak couplings at HERA and via strong coupling at the $p\bar{p}$ collider.

# References


[1] H1 collaboration, I. Abt et al, *Nucl. Phys.* B **396**, 3 (1993).

[2] H1 collaboration, T. Ahmed et al, *Phys. Lett.* B **340**, 205 (1994).

[3] H1 collaboration, S. Aid et al, *Nucl. Phys.* B **483**, 44 (1997).

[4] ZEUS collaboration, J. Breitweg et al, *Z. Phys.* C **76**, 631 (1997).

[5] DELPHI collaboration, P. Abreu et al, *Phys. Lett.* B **393**, 245 (1997).
L3 collaboration, M. Acciarri et al, *Phys. Lett.* B **401**, 139 (1997).

[6] OPAL collaboration, K. Ackerstaff et al, *Euro. Phys. Journal* C1, 45 (1998).
ALEPH collaboration, contribution to the EPS-HEP97 conference, Jerusalem (1997).

[7] L3 collaboration, contribution to ICHEP98, Vancouver, Abstract 498.

[8] CDF collaboration, F. Abe et al, *Phys. Rev.* D **55**, 5263 (1997).

[9] D0 collaboration, I. Bertram, FERMILAB-CONF-96/389-E.

[10] H1 Collaboration, I. Abt et al *Nucl. Instrum. Methods* A **386**, 310 and 348 (1997).

[11] H1 Calorimeter Group, B. Andrieu et al, *Nucl. Instrum. Methods* A **336**, 460 (1993).

[12] H1 Calorimeter Group, B. Andrieu et al, *Nucl. Instrum. Methods* A **344**, 492 (1994).

[13] H1 Calorimeter Group, B. Andrieu et al, *Nucl. Instrum. Methods* A **350**, 57 (1994) and *Nucl. Instrum. Methods* A **336**, 499 (1993).

[14] H1 SPACAL Group, R.D. Appuhn et al, *Nucl. Instrum. Methods* A **386**, 397 (1997).

[15] H1 BEMC Group, J. Ban et al, *Nucl. Instrum. Methods* A **372**, 399 (1996).

[16] DJANGO 6.2: G.A. Schuler and H. Spiesberger, Proc. of the Workshop Physics at HERA, Eds. W. Buchmüller, G.Ingelman, DESY Hamburg 1991,Vol 3, p 1419.

[17] HERACLES 4.4: A. Kwiatkowski, H. Spiesberger and H.-J. Möring, *Comp. Phys. Comm.* 69 (1992) 155.

[18] ARIADNE 4.0: L. Lönnblad, *Comp. Phys. Comm.* 71 (1992) 15.

[19] JETSET 7.3 and 7.4: T. Sjöstrand, Lund Univ. preprint LU-TP-95-20 (August 1995) 321pp; *idem*, CERN preprint TH-7112-93 (February 1994) 305pp.

[20] EPCOMPT: F. Raupach, Proc. of the Workshop Physics at HERA, Eds. W. Buchmüller, G. Ingelman, DESY Hamburg 1991,Vol 3, p 1473.

[21] COMPTON 2.0: A. Courau et al., Proc. of the Workshop Physics at HERA, Eds. W. Buchmüller, G. Ingelman, DESY Hamburg 1991,Vol 2, p 902 and Vol 3, p 1468.

[22] A.D. Martin, R.G. Roberts and W.J. Stirling, Proc. of the Workshop on Quantum Field Theoretical Aspects of High Energy Physics, ed. B. Geyser and E.M. Ilgenfritz, p.11 (1993).

[23] PYTHIA 5.7: T. Sjöstrand, CERN-TH-6488 (1992), *Comp. Phys. Comm.* 82 (1994)74.

[24] LPAIR: S. P Baranov et al., Proc. of the Workshop Physics at HERA, Eds. W. Buchmüller, G.Ingelman, DESY Hamburg 1991,Vol 3, p 1478.

[25] EPVEC: U. Baur, J.A.M Vermaseren, D. Zeppenfeld, *Nucl. Phys.* B **375**, 3 (1992).

[26] T. Köhler, Proc. of the Workshop Physics at HERA, Eds. W. Buchmüller, G.Ingelman, DESY Hamburg 1991, Vol 3, p 1526.

[27] K. Hagiwara, S. Komamiya and D. Zeppenfeld, *Z. Phys.* C **29**, 115 (1985).

[28] G. Jikia, *Nucl. Phys.* B **333**, 317 (1990).

[29] U. Baur, M. Spira and P. Zerwas, *Phys. Rev.* D **42**, 815 (1990).

[30] R. M. Barnett et al, *Phys. Rev.* D **54**, 1 (1996).

[31] ZEUS collaboration, M. Derrick, *Z. Phys.* C **65**, 627 (1995).

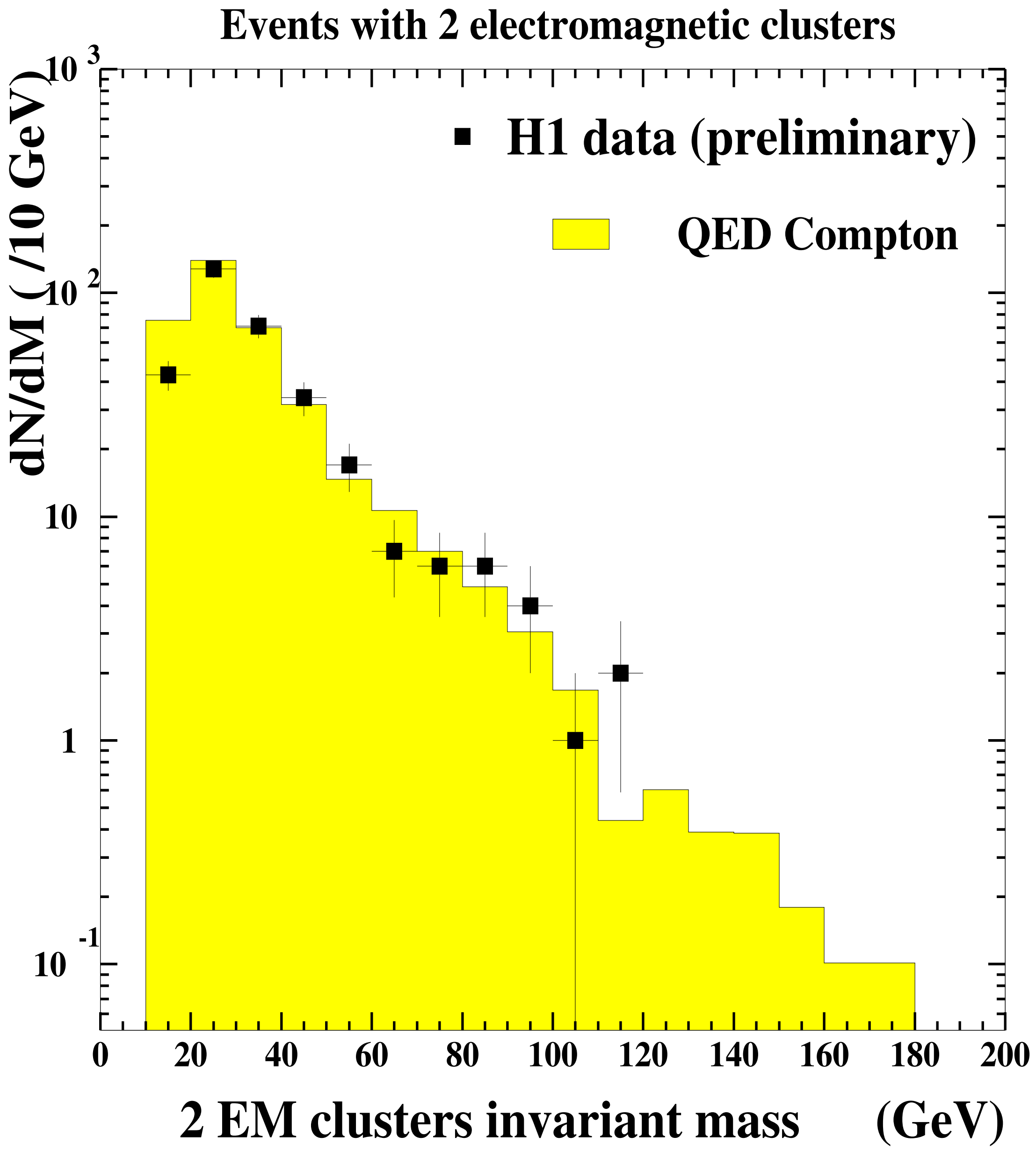


Figure 1: Invariant mass of the 2 electromagnetic clusters. Squares correspond to the data selected in the exclusive analysis and the histogram to the expected contribution of the QED Compton scattering normalized to the luminosity of the experiment.

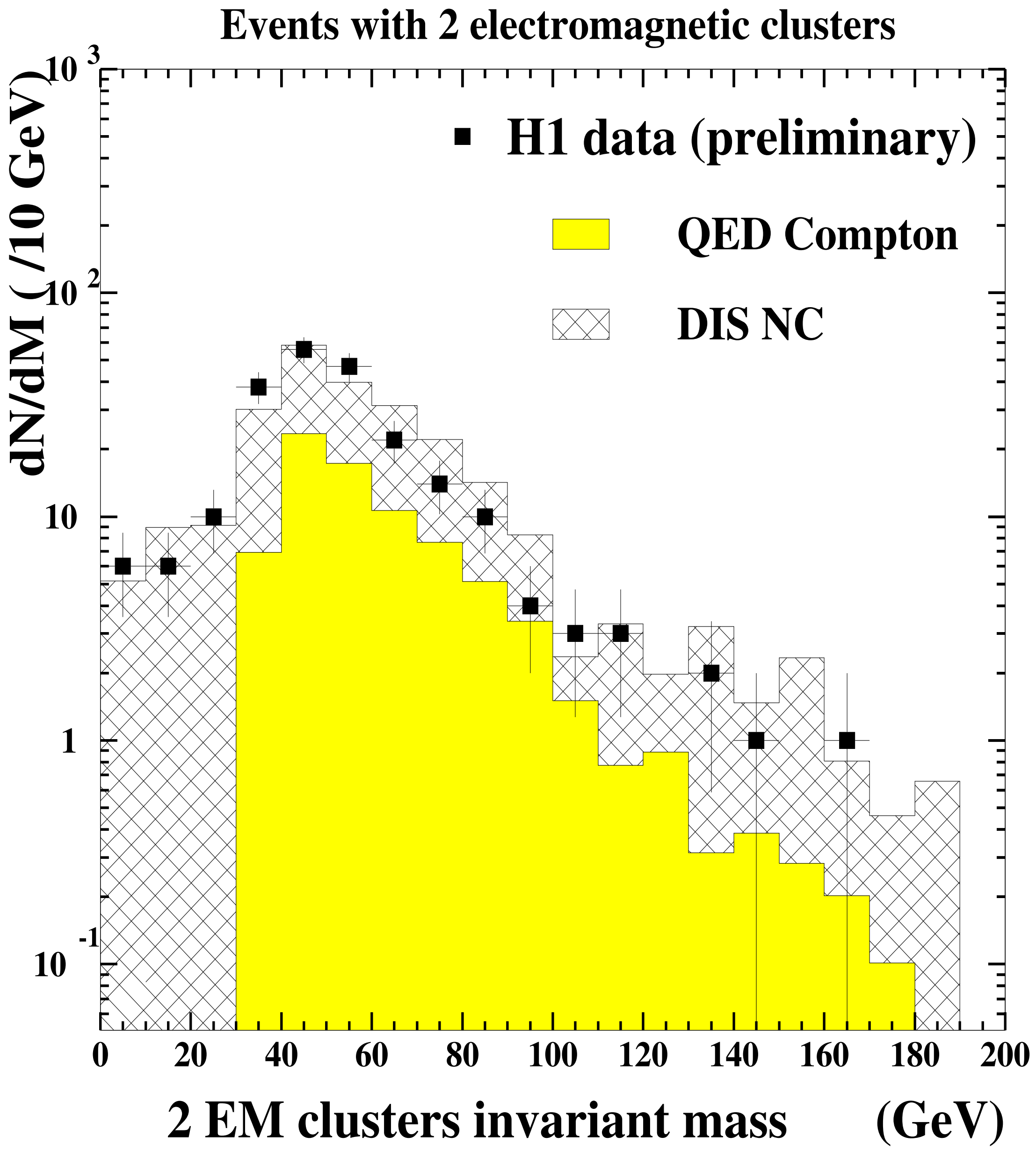


Figure 2: Invariant mass of the 2 electromagnetic clusters. Squares correspond to the data selected in the inclusive analysis and the histograms to the different expected contributions of Standard Model processes normalized to the luminosity of the experiment.

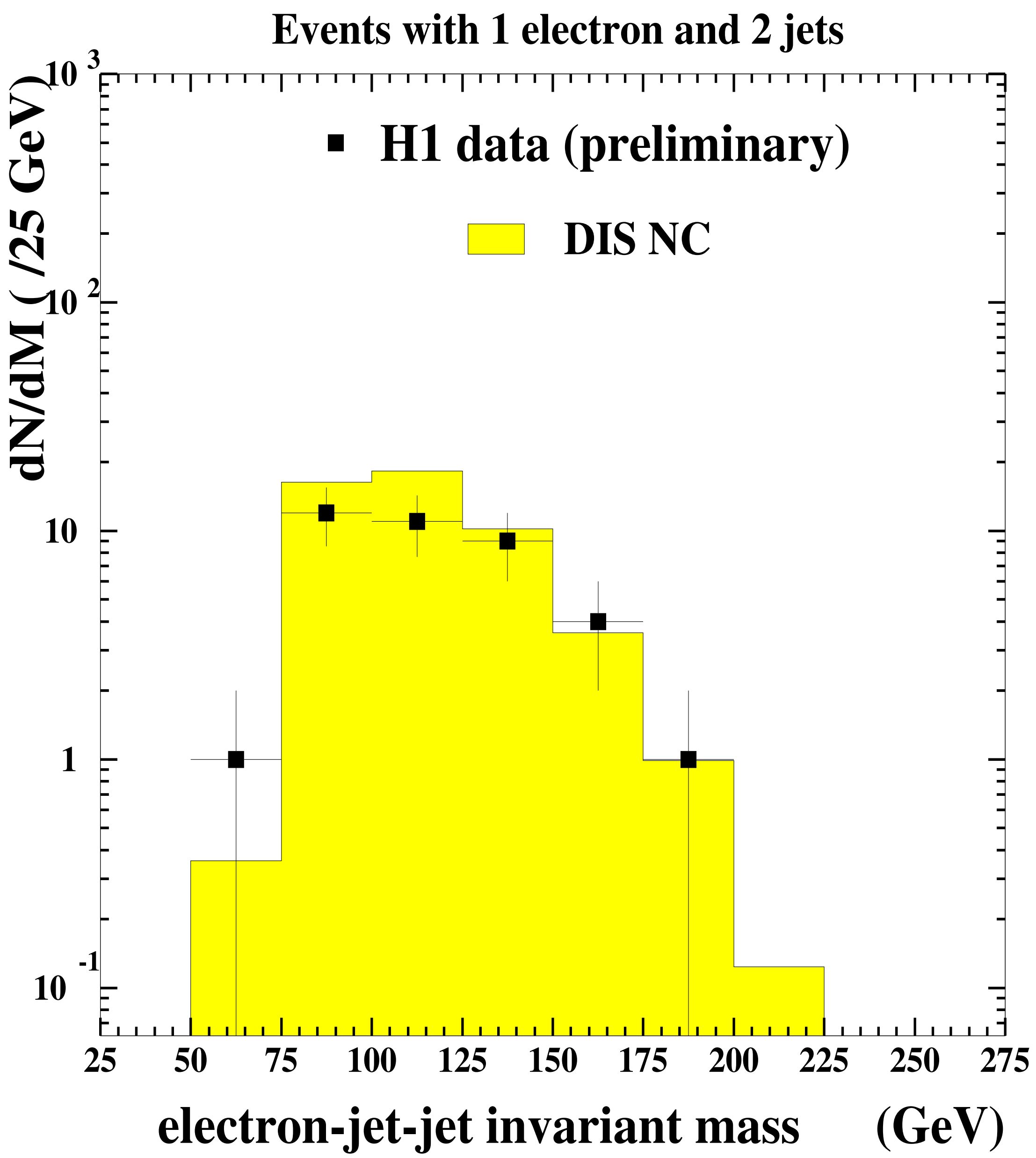


Figure 3: Invariant mass of the electromagnetic cluster and the 2 jets. Squares correspond to the data and the histogram to the expected contribution of the NC DIS process normalized to the luminosity of the experiment.

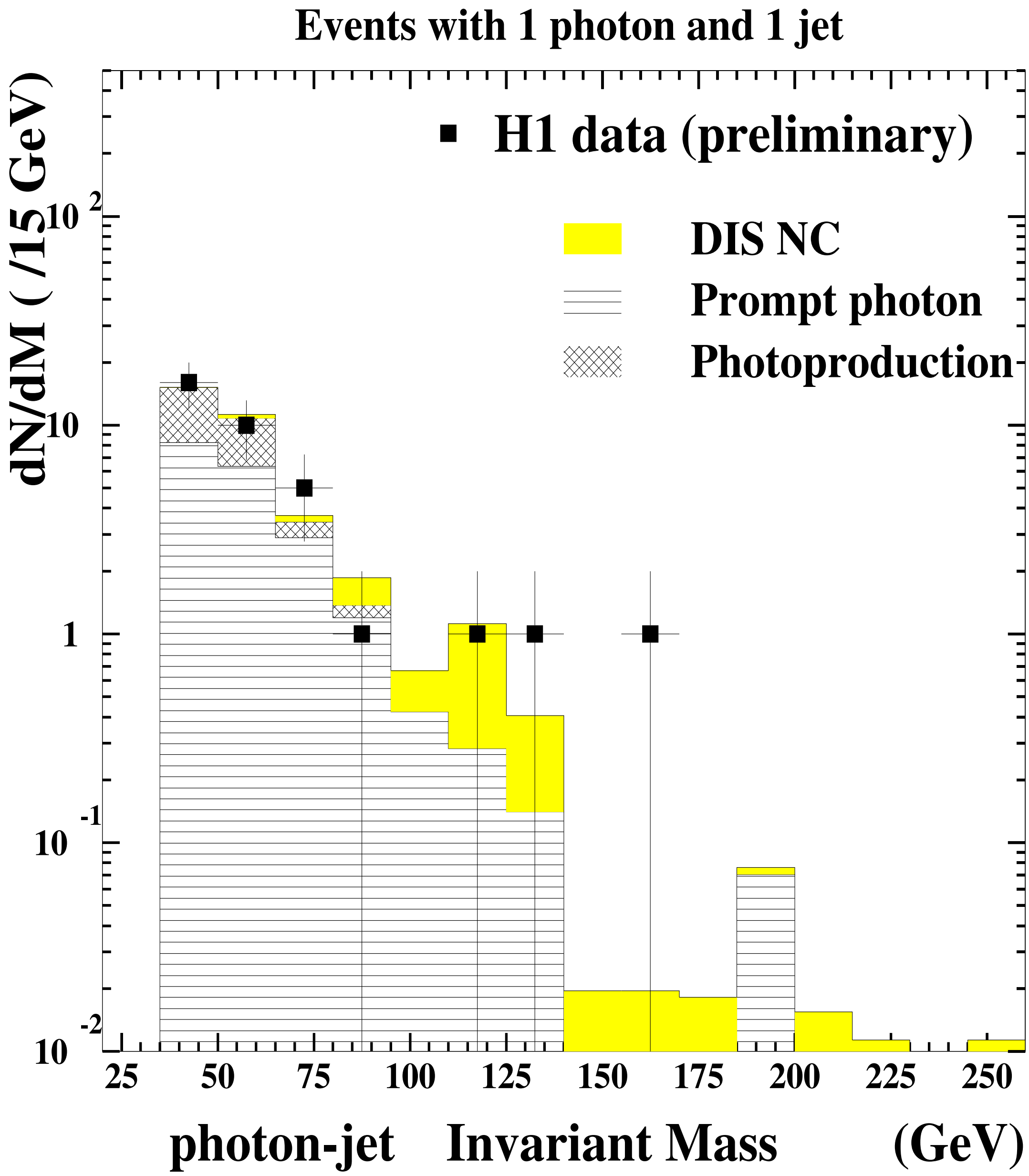


Figure 4: Invariant mass of the electromagnetic cluster and the jet. Squares correspond to the data and the histograms to the different expected contributions of Standard Model processes normalized to the luminosity of the experiment.

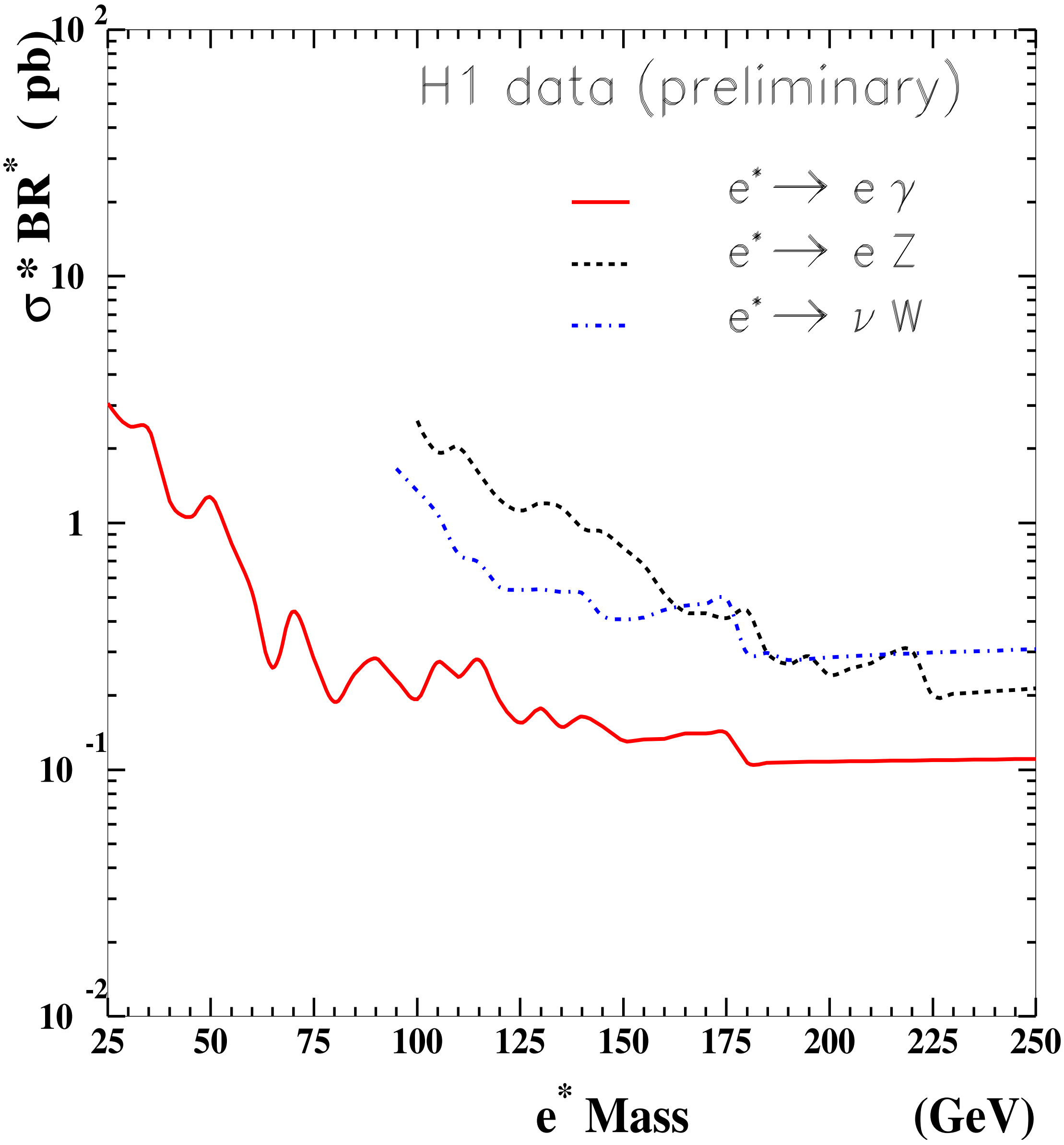


Figure 5: Upper limits at the $95\%$ confidence level on the product of the cross section and the decay channel branching ratio for excited electron production. The full line corresponds to the $e^*$ radiative decay, the dashed and dotted-dashed lines to the $e^* \to eZ$ and the $e^* \to \nu W$ decays respectively. Decay channels of the gauge boson $W$ and $Z$ are combined. Areas above the curves are excluded.

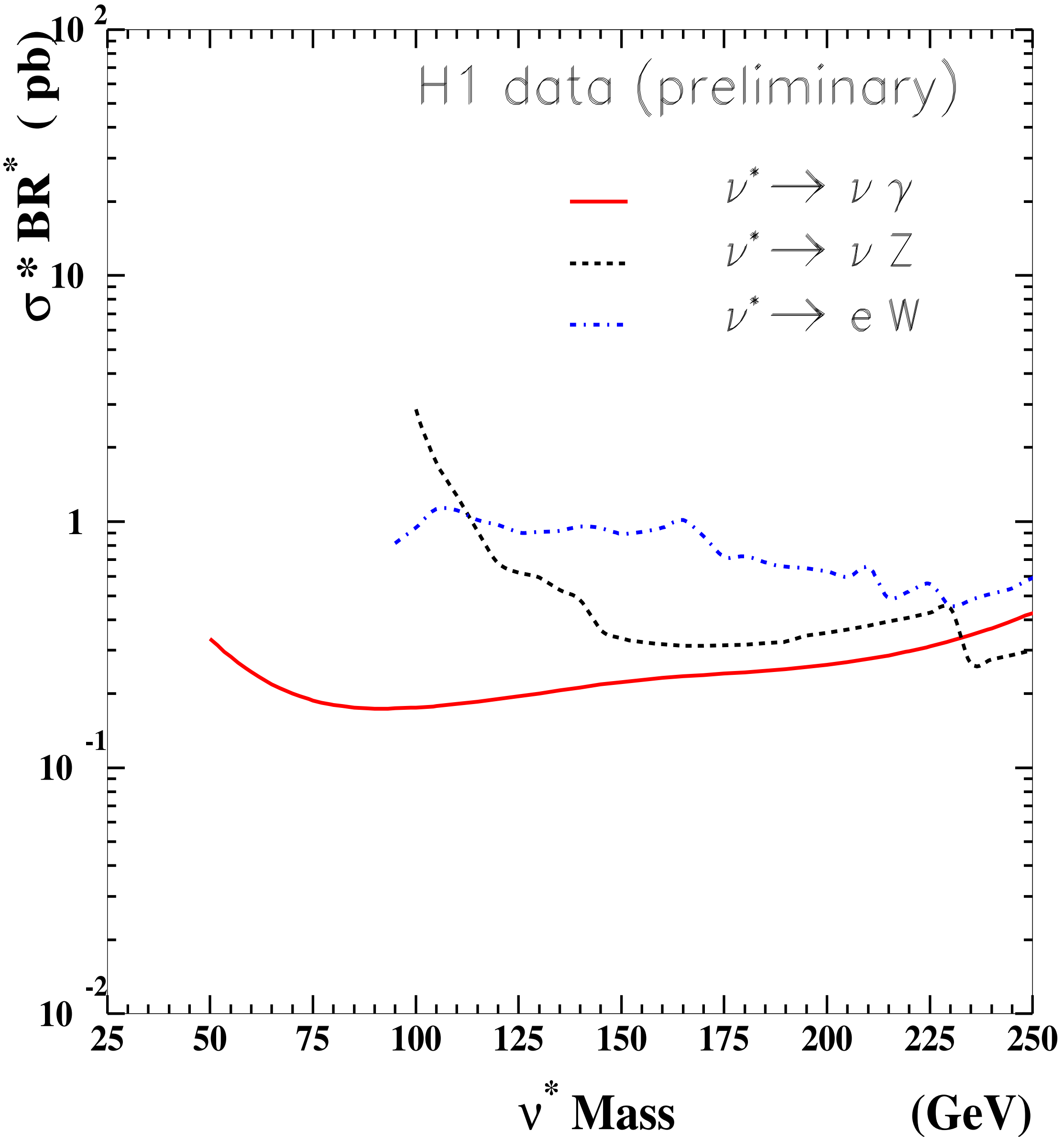


Figure 6: Upper limits at the 95% confidence level on the product of the cross section and the decay channel branching ratio for excited neutrino production. The full line corresponds to the $\nu^*$ radiative decay, the dashed and dotted-dashed lines to the $\nu^* \rightarrow \nu Z$ and the $\nu^* \rightarrow eW$ decays respectively. Decay channels of the gauge boson $W$ and $Z$ are combined. Areas above the curves are excluded.

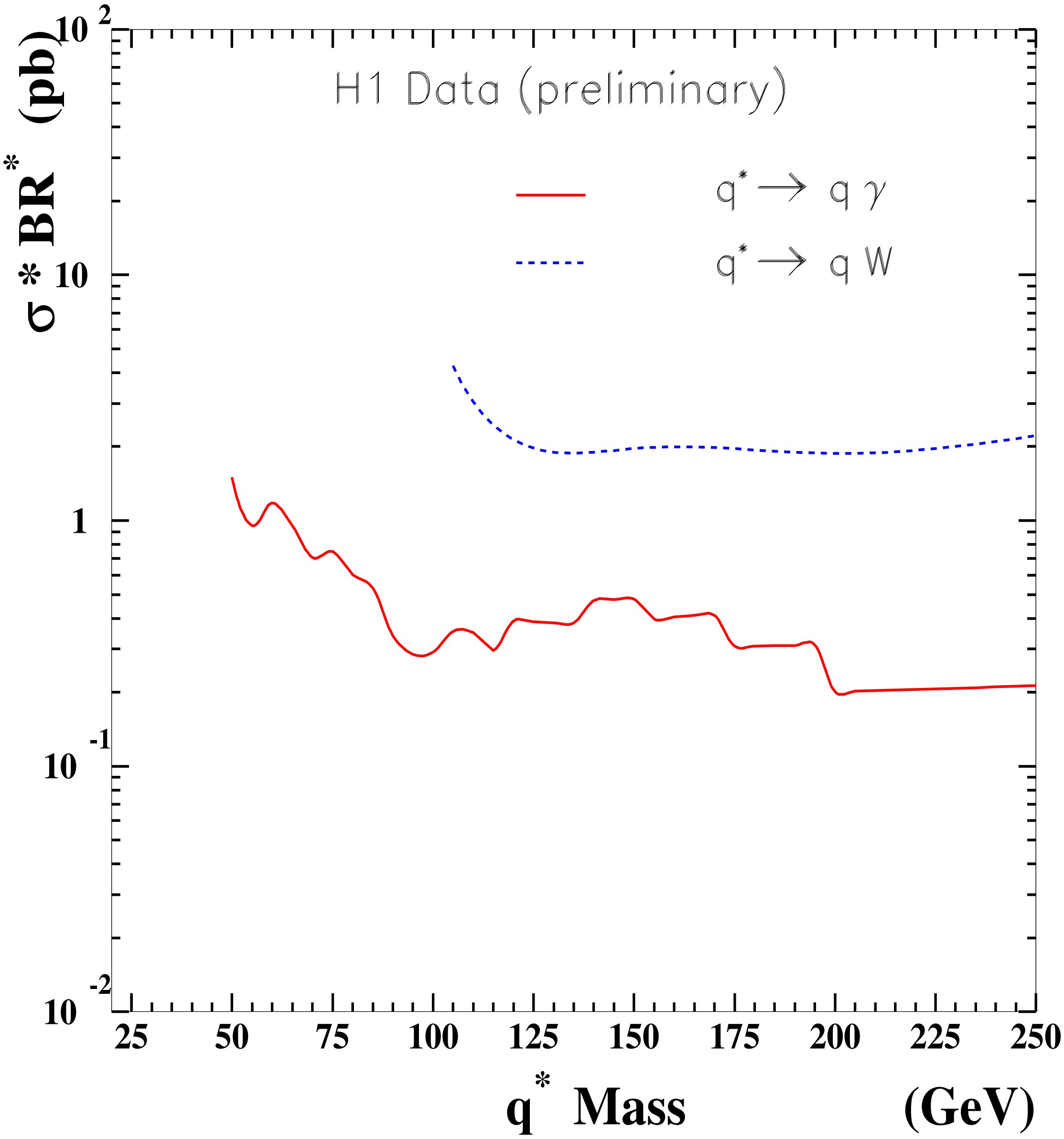


Figure 7: Upper limits at the $95\%$ confidence level on the product of the cross section and the decay channel branching ratio for excited quark production in the electromagnetic (full line) and $W$ (dashed line) decay channels. Areas above the curves are excluded.

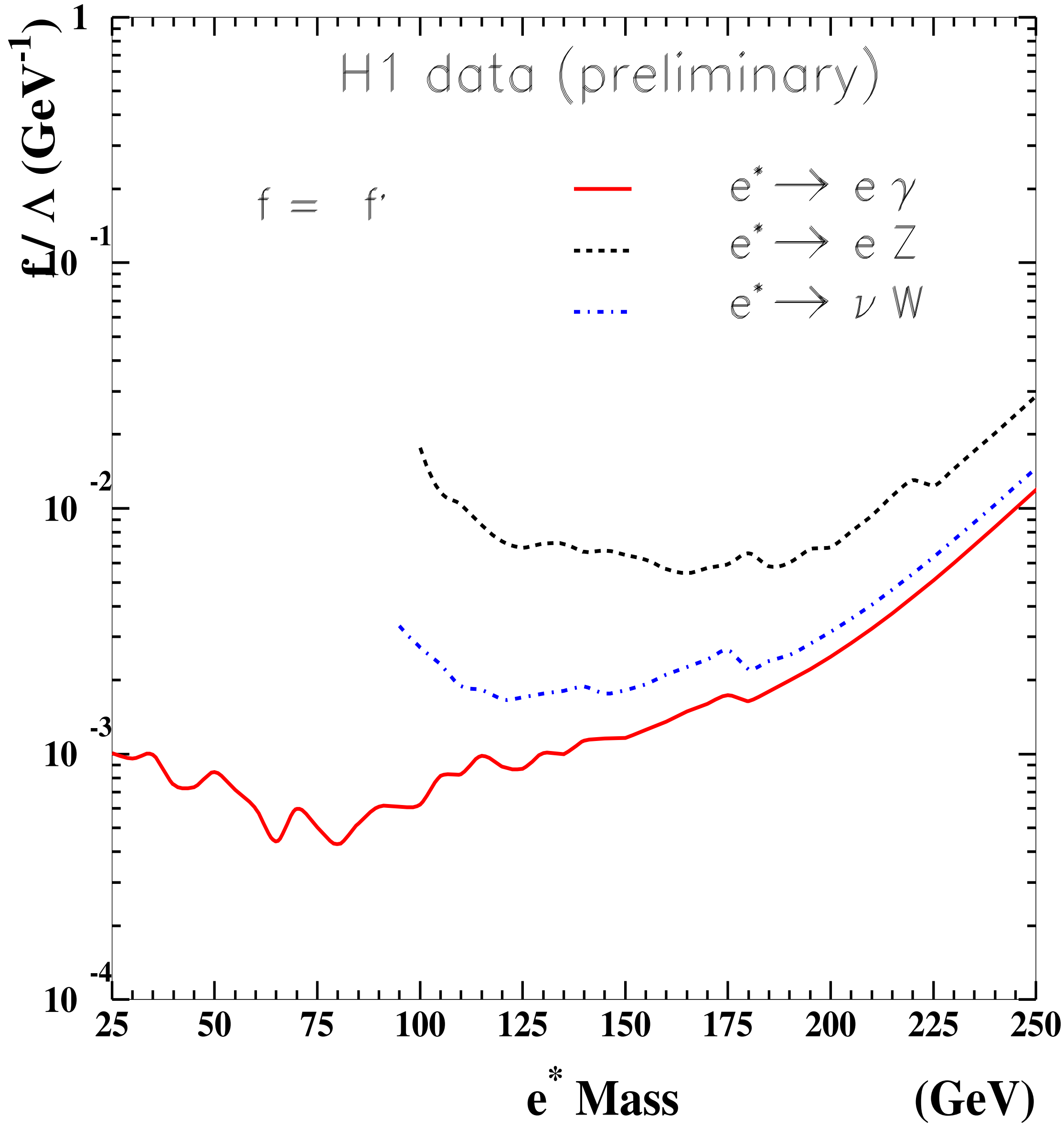


Figure 8: Exclusion limits on coupling constants at the $95\%$ confidence level as a function of the mass for excited electron production. The assumption $f = f'$ is made for the different decay channels (full line for radiative, dashed line for $Z$ and dotted-dashed line for $W$ decays). Values of the couplings above the curves are excluded.

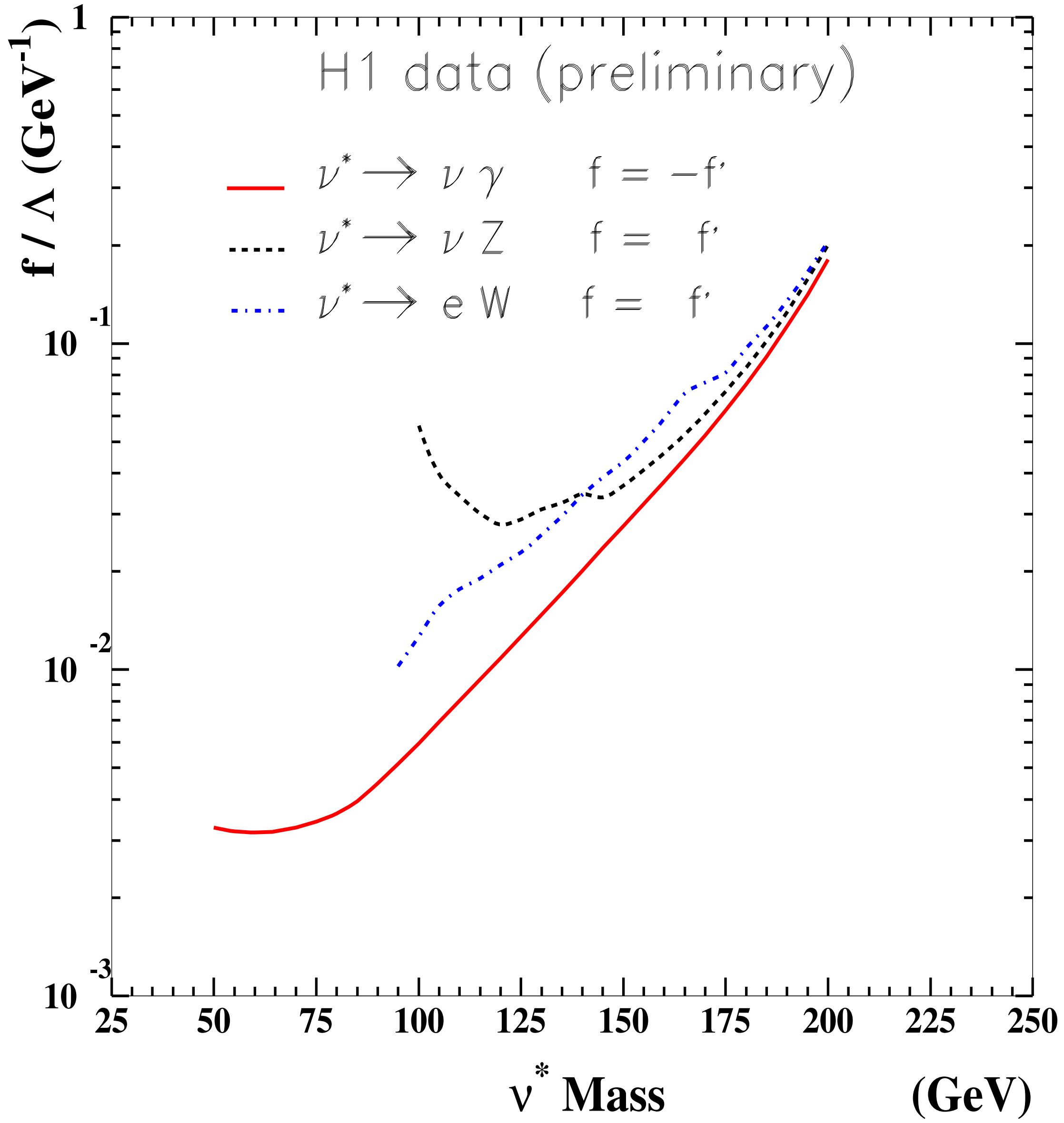


Figure 9: Exclusion limits on coupling constants at the $95\%$ confidence level as a function of the mass for excited neutrino production. The relation $f = f'$ is assumed for the decays involving a $Z$ or a $W$ (dashed line for the $Z$ and dotted-dashed line for the $W$) and $f = -f'$ for the radiative decay (full line). Values of the couplings above the curves are excluded.

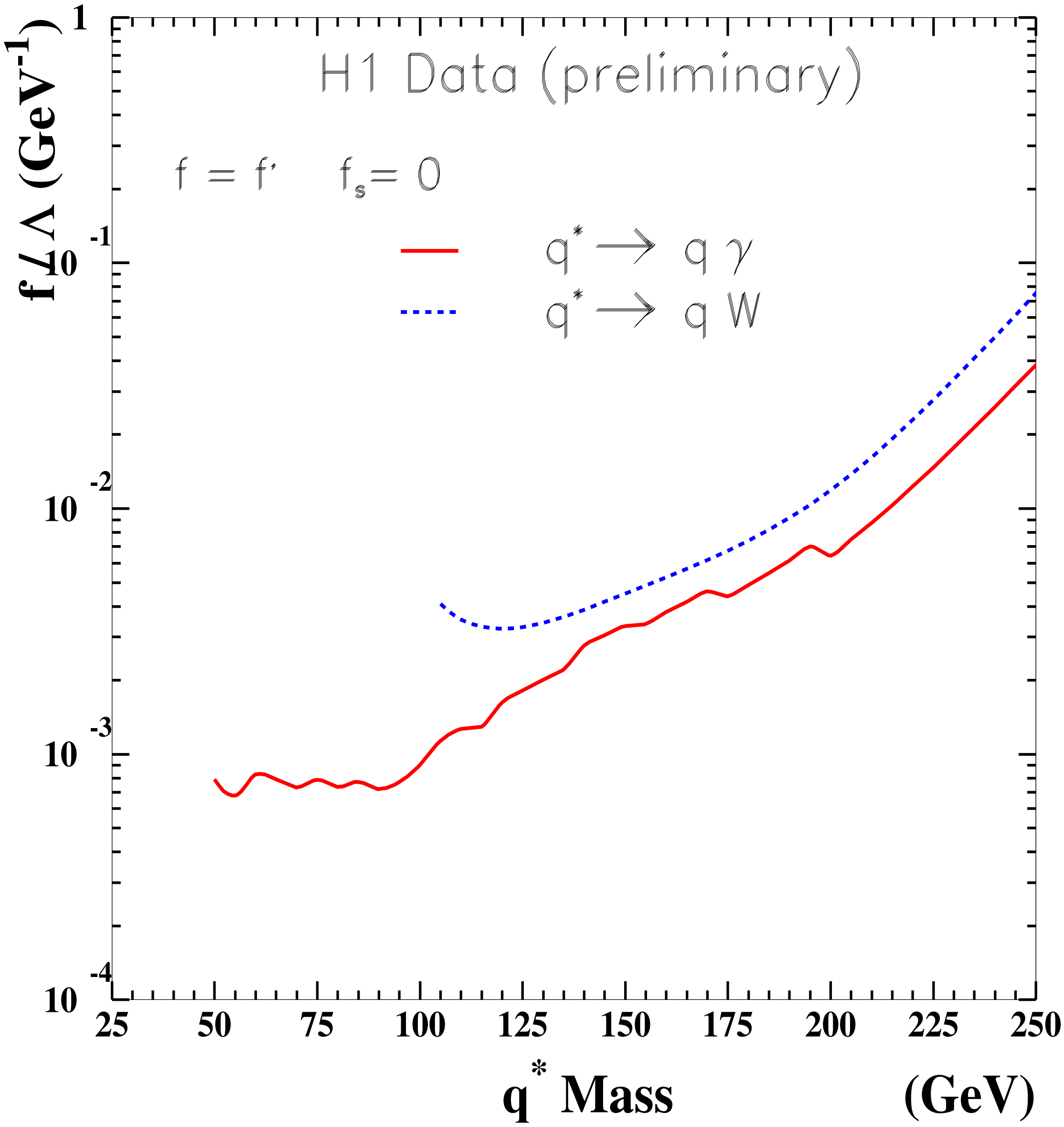


Figure 10: Exclusion limits on coupling constants at the $95\%$ confidence level as a function of the mass for excited quark production, assuming $f = f'$ and $f_s = 0$. The radiative decay is shown in full line and the $W$ decay in dashed line. Values of the couplings above the curves are excluded.

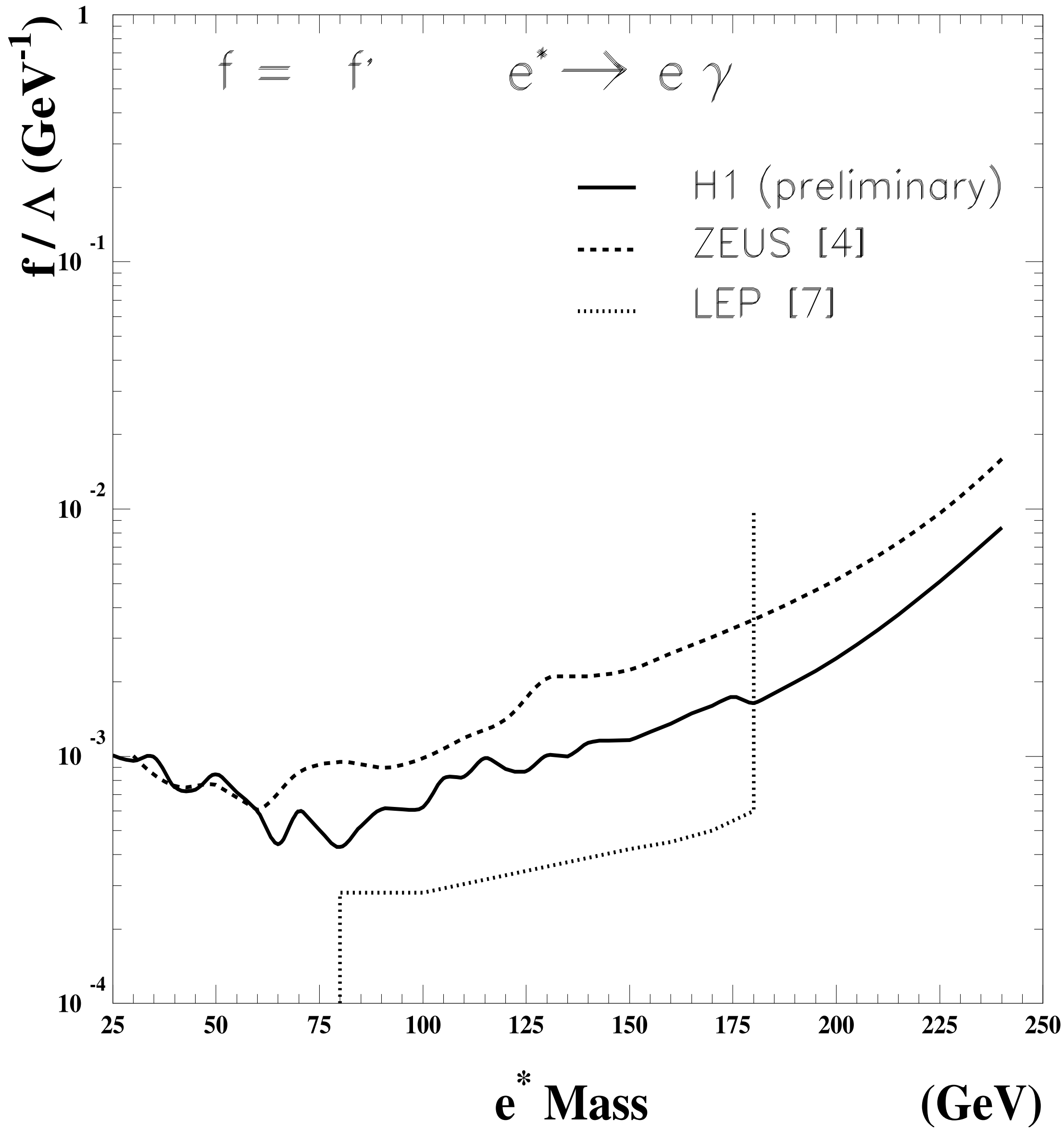


Figure 11: Comparison of the limits on the coupling constants at the $95\%$ confidence level from H1, ZEUS and LEP for the $e^{*}$. H1 and ZEUS [4] limits are represented in full line and dashed line respectively. The dotted line stands for the L3 experiment result [7].

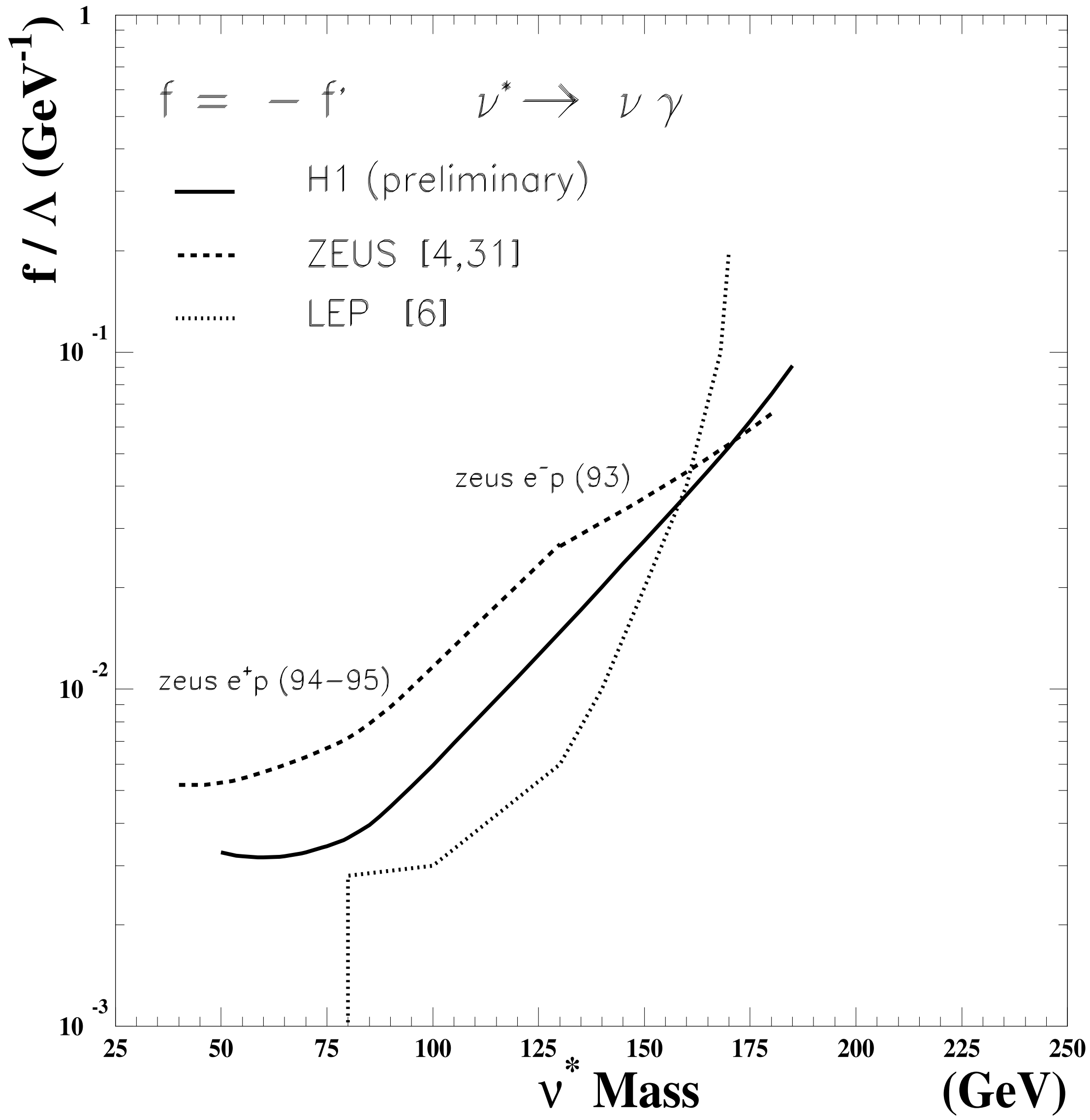


Figure 12: Comparison of the limits on the coupling constants at the $95\%$ confidence level from H1, ZEUS and LEP for the $\nu^*$. H1 and ZEUS [4, 31] limits are represented in full and dashed line respectively. The dotted line stands for the OPAL-ALEPH experiment results [6].

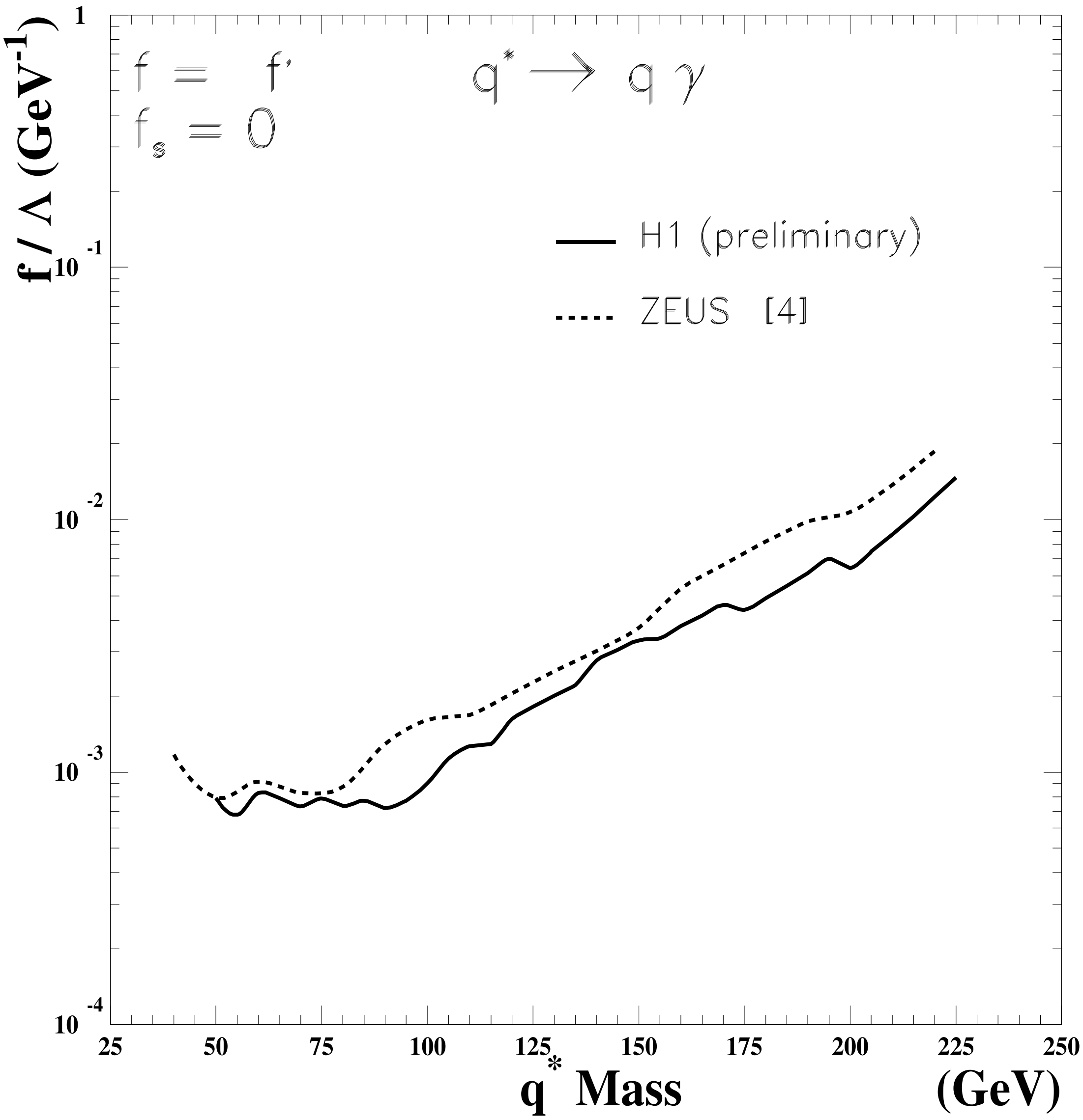


Figure 13: Comparison of the limits on the coupling constants at the 95% confidence level from H1 and ZEUS for the $q^*$. H1 and ZEUS [4] limits are represented in full and dashed line respectively.